An image domain approach to the interpretation of the visible moiré phenomenon

2013 J. Opt. 15 075407

(http://iopscience.iop.org/2040-8986/15/7/075407)

IOP Publishing Journal of Optics
J. Opt. **15** (2013) 075407 (11pp) doi:10.1088/2040-8978/15/7/075407

An image domain approach to the interpretation of the visible moiré phenomenon

Lei Yu, Shu-rong Wang and Guan-yu Lin

Institute of Optics, Fine Mechanics and Physics, Chinese Academy of Sciences, Changchun 130033, People's Republic of China

E-mail: top1gods@mail.ustc.edu.cn (S-R Wang)

Received 23 April 2013, accepted for publication 10 June 2013
Published 27 June 2013
Online at stacks.iop.org/JOpt/15/075407

Abstract
An approach to the interpretation of the visible moiré phenomenon in the image domain has been proposed. The analysis of the Fourier series expansion presents an initial criterion for distinguishing the real moiré and pseudo-moiré cases. A geometric calculation of the superposed grating lines is utilized to obtain the parameters for describing the real and pseudo-moiré cases. On the basis of the study, the average intensities of the waveforms of the real moiré and pseudo-moiré cases are calculated in order to provide the interpretation. It indicates that different moiré cases result from the garbled discernment of human eyes, which is introduced by the microstructure versus macrostructure effects. The variations of intensity and average intensity in the microstructure result in the confusion of the average intensities of the real moiré and pseudo-moiré waveforms. The interpretation is significant for the visible real and pseudo-moiré effects, both in the multiplicative superposition and in the additive superposition composed from periodic cosinusoidal gratings and binary gratings in the image domain. The approach also considers the coexistence of the real moiré and pseudo-moiré cases. The rule for their coexistence has been summarized in the image domain.

Keywords: moiré, Fourier analysis, grating

(Some figures may appear in colour only in the online journal)

1. Introduction

The moiré phenomenon occurs when periodic or repetitive structures are superposed. It has been well known for a long time, since it was found at first in France, exhibited by water silk. Generally, the superposition of two or more periodic (or quasi-periodic) structures leads to a coarser structure, which is the appearance of interfering patterns, named moiré patterns or moiré fringes [1].

The moiré fringe technique is a well-established tool in optical metrology [2, 3]. The first scientific observations were made by Lord Rayleigh [4], who suggested using the moiré phenomenon for testing the quality of gratings. In modern moiré pattern research, there are two aspects which are the analysis of moiré patterns and moiré pattern synthesis. The two parts are tightly linked and understanding one gives insight into the other [5]. The modern moiré theory is largely based on the Fourier approach [6].

There is an interesting phenomenon called the pseudo-moiré phenomenon, and it seems that the Fourier theory by itself cannot answer all the questions relating to it [7, 8]. The pseudo-moiré phenomenon is one that the human eyes can receive, but the Fourier theory cannot capture. In other words, the moiré case is considered non-existent in Fourier theory. Isaac Amidror gave the basic combination of points in the theoretical prediction of visible moiré effects [9]: the effect of non-linearities; microstructure versus macrostructure effects; the human visual system; modulation. Kong [10] interpreted the phenomenon with the consideration of the illusional contrast of the human visual system. Patorski [11] used the

concept of biased and unbiased frequency pairs to interpret the real and pseudo-moiré cases in the Fourier domain on the basis of the notion of detectable intensity modulations. In his method, the moiré pattern characteristics can be readily predicted by the continuous wavelet transform and fast adaptive bidimensional empirical mode decomposition methods.

The interpretation in this paper is presented for the visible moiré phenomenon in the image domain. In section 2, the Fourier expansion is utilized to study the generation of the moiré effect. The geometric method for periodic gratings is used to calculate parameters for the real moiré and pseudo-moiré cases in the multiplicative superposition. The calculation of the average intensity of the moiré effect shows that the microstructure versus the macrostructure effect introduces confusion to human eyes in different ratios of equivalent periods. It also proves the coexistence of the real moiré and pseudo-moiré cases. In section 3, similar interpretations and calculations are used for the multiplicative superposition of binary gratings and display favorable rationality. In section 4, an interpretation is applied for the additive superposition. And we supply some corrections to accommodate the interpretation to binary gratings. In section 5, the regularity of the real moiré and pseudo-moiré coexistence is summarized by giving examples.

2. Theoretical interpretation for the multiplicative superposition of cosinusoidal gratings

For the sake of simplicity and clarity of presentation, we only study the superposition composed of two periodic gratings in the following sections.

2.1. Description of the generated moiré case from the Fourier expansion

The expression for the cosinusoidal gratings is as follows:

$$r_i = \tfrac{1}{2}\cos[2\pi f_i(x\cos\theta_i + y\sin\theta_i)] + \tfrac{1}{2}. \tag{1}$$

Using a vector notation, the generalization of formula (1) to the 2D case is

$$\vec{r_i} = \tfrac{1}{2}\cos(2\pi\,\vec{f_i}\cdot\vec{x}) + \tfrac{1}{2}, \qquad \text{where}$$
$$\vec{f_i} = f_i(\cos\theta_i, \sin\theta_i), \quad \vec{x} = (x, y). \tag{2}$$

An arbitrary periodic even function which satisfies the Dirichlet theorem can be expressed in the form of a Fourier expansion:

$$f(x) = \frac{a_0}{2} + \sum_{n=1}^{\infty} a_n \cos 2n\pi\,\vec{f}\,\vec{x},$$
$$\left(a_n = 4\,\vec{f}\int_0^{\frac{1}{2\vec{f}}} f(\vec{x})\cos 2n\pi\,\vec{f}\,\vec{x}\,\mathrm{d}\,\vec{x}\,(n = 1, 2, 3, \ldots)\right). \tag{3}$$

The multiplicative superposition $r_1(x, y) \times r_2(x, y)$ can be expressed as

$$\begin{aligned} r_1 \times r_2 = \frac{1}{2}\Bigg[& \frac{a_0^1 a_0^2}{2} + a_0^1 \sum_{n=1}^{\infty} a_n^1 \cos 2n\pi\,\vec{f_1}\,\vec{x} \\ & + a_0^2 \sum_{n=1}^{\infty} a_m^2 \cos 2m\pi\,\vec{f_2}\,\vec{x} + \sum_{n=1}^{\infty}\sum_{m=1}^{\infty} a_n^1 a_m^2 \\ & \times \cos 2\pi(n\vec{f_1} + m\vec{f_2})\,\vec{x} + \sum_{n=1}^{\infty}\sum_{m=1}^{\infty} a_n^1 a_m^2 \\ & \times \cos 2\pi(n\vec{f_1} - m\vec{f_2})\,\vec{x}\Bigg], \end{aligned} \tag{4}$$

where

$$a_0^1 = a_0^2 = 1, \qquad a_n^1 = \begin{cases} \frac{1}{2} & (n = 1) \\ 0 & (n > 1) \end{cases},$$

$$a_m^2 = \begin{cases} \frac{1}{2} & (m = 1) \\ 0 & (m > 1) \end{cases}.$$

The $(k_1, \pm k_2)$ moiré terms are isolated by the last two generated terms:

$$m_{k_1,\pm k_2} = \tfrac{1}{2}\sum_{n'=1}^{\infty} a_{n'k_1}^1 a_{n'k_2}^2 \cos 2\pi n'(k_1\vec{f_1} \pm k_2\vec{f_2})\,\vec{x}\,. \tag{5}$$

There is another form of $r_1 \times r_2$ from expression (1):

$$\begin{aligned} r_1 \times r_2 = {} & \tfrac{1}{4}\left[1 + \cos(2\pi\,\vec{f_1}\cdot\vec{x}) + \cos(2\pi\,\vec{f_2}\cdot\vec{x})\right] \\ & + \tfrac{1}{8}(\cos[2\pi(\vec{f_1} + \vec{f_2})\,\vec{x}] + \cos[2\pi(\vec{f_1} - \vec{f_2})\,\vec{x}]). \end{aligned} \tag{6}$$

The $(k_1, \pm k_2)$ moiré terms isolated from (6) are

$$m_{k_1,\pm k_2} = \tfrac{1}{8}\cos[2\pi(\vec{f_1} + \vec{f_2})\,\vec{x}] + \tfrac{1}{8}\cos[2\pi(\vec{f_1} - \vec{f_2})\,\vec{x}]. \tag{7}$$

In contrast to the case for formulas (5) and (7), it can be found that there only exist non-zero $(1, \pm 1)$ moiré terms in the expression for the superposition. When $k_1 \neq \pm 1$ or $k_2 \neq \pm 1$, the coefficients of the new generated terms are zero. So the amplitudes of the generated impulses of these terms are zero. The Fourier analysis will not capture these impulses, but the effect of these terms may be received by the human visual system. It presents a concise initial criterion for the real moiré and the pseudo-moiré cases. Namely, if terms of the corresponding moiré phenomenon which are not equal to 0 (the coefficients $k_1 \neq \pm 1$ or $k_2 \neq \pm 1$) are received by human eyes, this will be the pseudo-moiré phenomenon.

2.2. Calculation of parameters of the real and pseudo-moiré phenomena in the image domain

The calculation will be performed to obtain the parameters of the real moiré and the pseudo-moiré phenomena and illustrate their governing factors. Our analysis only involves the image domain in figure 1.

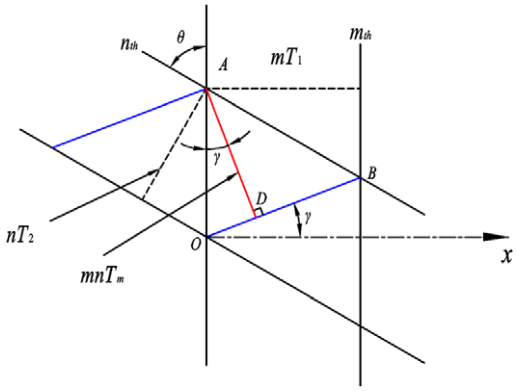

Figure 1. Geometric analysis of the moiré phenomenon in the multiplicative superposition.

The periods of two gratings are T_1 and T_2, and θ is their included angle. The superposition of two gratings generates the (m, n) line family. The blue line OB stands for one line of the generated line family. The line family can be actually considered as a new generated $(n, \pm m)$ moiré case. It is assumed that the period of the (m, n) line family is T_m, which is also the length of the interval between two adjacent lines. The two blue lines in figure 1 are generated by the mth line in grating r_1 and the nth line in grating r_2, so the length of AD is mnT_m. The included angle between OB and the x axis is γ, which defines the direction of the (m, n) line family. These two parameters T_m, n and $\cos\gamma$ can describe the generated line family (namely, the moiré phenomenon) sufficiently. It is denoted by $T_1 \leq T_2$, for the reciprocity between them.

The parameter $\cos\gamma$ will be primarily calculated according to the law of cosines in the triangle ABO, where $\mathrm{OB} = mT_1/\cos\gamma$, $\mathrm{AO} = nT_2/\sin\theta$, and $\mathrm{AB} = mT_1/\sin\theta$:

$$\begin{aligned}\cos\gamma &= \frac{mT_1}{\sqrt{\mathrm{AO}^2 + \mathrm{AB}^2 - 2\mathrm{AO}\cdot\mathrm{AB}\cdot\cos\theta}} \\ &= \frac{mT_1\sin\theta}{\sqrt{m^2T_1^2 + n^2T_2^2 - 2mnT_1T_2\cos\theta}}.\end{aligned} \tag{8}$$

In the right-angle triangle AOD, the period is expressed as

$$\begin{aligned}T_{m,n} &= \frac{\mathrm{AO}\cdot\cos\gamma}{mn} \\ &= \frac{T_1T_2}{\sqrt{m^2T_1^2 + n^2T_2^2 - 2mnT_1T_2\cos\theta}}.\end{aligned} \tag{9}$$

Besides the calculation, the following relationship is also obtained in the analysis:

$$\mathrm{OB} = \frac{mT_1}{\cos\gamma} = \frac{nT_2}{\cos(\theta-\gamma)}. \tag{10}$$

It presents the equivalent periods of r_1 and r_2 along the direction OB:

$$\frac{T_1'}{T_2'} = \frac{T_1/\cos\gamma}{T_2/\cos(\theta-\gamma)} = \frac{n}{m}. \tag{11}$$

(1) Real moiré cases ($m = \pm n$, $(1, \pm 1)$ moiré cases).

According to the moiré coefficient calculation in section 2.1, the $(1, \pm 1)$ moiré case is the real moiré case. At the moment we have $T_1'/T_2' = \pm 1$. The parameters of the real moiré case are

$$\begin{aligned}\cos\gamma_\mathrm{r} &= \frac{T_1\sin\theta}{\sqrt{T_1^2 + T_2^2 \mp 2T_1T_2\cos\theta}}, \\ T_\mathrm{r} &= \frac{T_1T_2}{\sqrt{T_1^2 + T_2^2 \mp 2T_1T_2\cos\theta}}.\end{aligned} \tag{12}$$

(2) Pseudo-moiré cases ($m \neq n$, $(n, \pm m)$ moiré cases).

In this situation, $(T_1/\cos\gamma_\mathrm{p})/(T_2/\cos(\theta-\gamma_\mathrm{p})) = \pm n/m$. The parameters of the pseudo-moiré case are

$$\begin{aligned}\cos\gamma_\mathrm{p} &= \frac{mT_1\sin\theta}{\sqrt{m^2T_1^2 + n^2T_2^2 \mp 2mnT_1T_2\cos\theta}}, \\ T_\mathrm{p} &= \frac{T_1T_2}{\sqrt{m^2T_1^2 + n^2T_2^2 \mp 2mnT_1T_2\cos\theta}}.\end{aligned} \tag{13}$$

2.3. The heuristic interpretation of the physical meaning

An appropriate interpretation for the moiré phenomenon will be given based on the above analysis. To make our interpretation clearer, a three-dimensional datagram is used in figure 2.

The values on the Z axis distributing in the interval [0, 1] are the values of the reflectance function for any point (x, y) of the grating, which represents its intensity: 0 for black, 1 for white and the intermediate value between them. There is an inclined angle $\pi/10$ between the gratings r_1 and r_2. The vertical cross-section of r_1 is parallel to the plane XZ. According to the parameter calculated in the last section, two waveforms in the cross-sections along the direction $\cos\gamma_\mathrm{r}$ and $\cos\gamma_\mathrm{p}$ are obtained in figures 2(f) and (g). They stand for the new generated waveforms of the real and pseudo-moiré cases. Then the average intensities of these waveforms will be calculated. To make the calculation more illustrative and clearer, the 2D case will be notated in the 1D form as in section 2.1. The waveform r' in the cross-section of $r_1 \times r_2$ along the moiré direction can be expressed as the product of the two waveforms of r_1' and r_2', which are the projections of r_1 and r_2 at the same cross-section. These two projections of waveforms can be expressed in the 1D case as

$$\begin{cases} r_1' = \dfrac{1}{2}\cos\left(\dfrac{2\pi}{\vec{T}_1'}\vec{x}\right) + \dfrac{1}{2} \\ r_2' = \dfrac{1}{2}\cos\left(\dfrac{2\pi}{\vec{T}_2'}\vec{x} + \delta\right) + \dfrac{1}{2}, \end{cases} \tag{14}$$

where $\vec{T}_1' = \vec{T}_1/\cos\gamma$, $\vec{T}_2' = \vec{T}_2/\cos(\theta-\gamma)$, which are the equivalent periods of r_1' and r_2'. δ is the angular displacement along the new $\boldsymbol{X}$ axis.

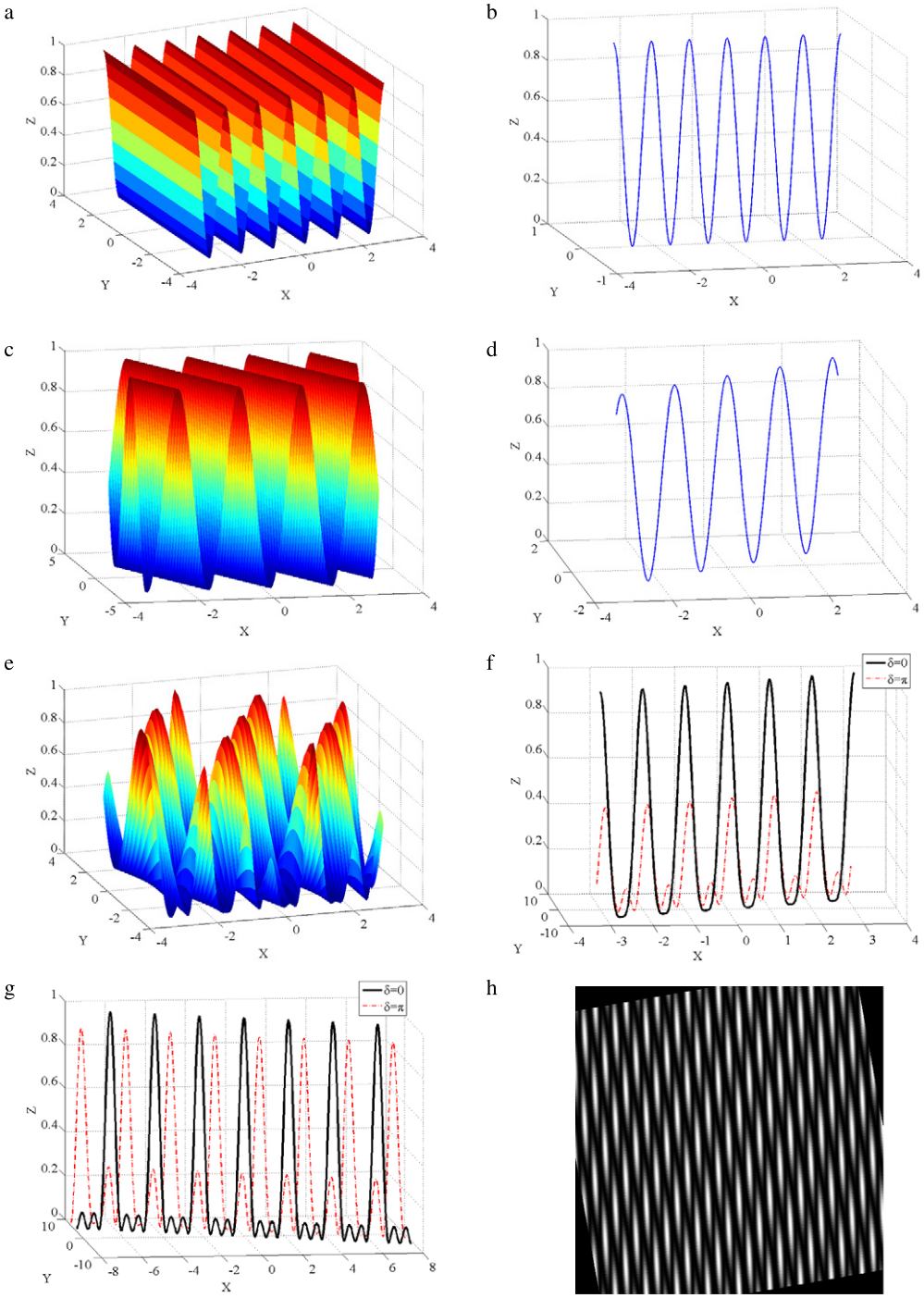

Figure 2. The oscillograms and the waveforms in the vertical cross-section of the gratings and their multiplicative superposition where $r_1 = 1/2\cos[4(x\cos(0) + y\sin(0))] + 1/2$, $r_2 = 1/2\cos[6(x\cos(\pi/10) + y\sin(\pi/10))] + 1/2$. (a) The three-dimensional wave profile of r_1. (b) The waveform in the vertical cross-section of r_1. (c) The three-dimensional wave profile of r_2. (d) The waveform in the vertical cross-section of r_2. (e) The three-dimensional wave profile of $r_1 \times r_2$. (f) Waveforms in the vertical cross-section along $\cos\gamma_r$ of $r_1 \times r_2$. (g) Waveforms in the vertical cross-section along $\cos\gamma_p$ of $r_1 \times r_2$. (h) The superposition image of the gratings.

The waveform r' in any arbitrary parallel cross-section of the real or the pseudo-moiré case can be expressed as the product of r'_1 and r'_2:

$$r' = r'_1 \times r'_2 = \frac{1}{4} + \frac{1}{4}\cos\left(\frac{2\pi}{\vec{T}'_1}\vec{x}\right) + \frac{1}{4}\cos\frac{2\pi}{\vec{T}'_2}(\vec{x}+\delta) + \frac{1}{8}\left[\cos 2\pi\left(\frac{\vec{T}'_1+\vec{T}'_2}{\vec{T}'_1\vec{T}'_2}\right)\left(\vec{x}+\frac{\vec{T}'_1}{\vec{T}'_1+\vec{T}'_2}\delta\right) + \cos 2\pi\left(\frac{\vec{T}'_1+\vec{T}'_2}{\vec{T}'_1\vec{T}'_2}\right)\left(\vec{x}-\frac{\vec{T}'_1}{\vec{T}'_2-\vec{T}'_1}\delta\right)\right]. \quad (15)$$

The average intensity of r' will be obtained by the integral method using the expression (15).

(1) The real moiré case:

According to the analysis in section 2.2, $\vec{T}'_1 / \vec{T}'_2 = 1$, so $\vec{T}' = \vec{T}'_1 = \vec{T}'_2$. Then the waveform of expression (15) can be expressed as

$$r' = \frac{1}{4} + \frac{1}{4}\cos\left(\frac{2\pi}{\vec{T}'}\vec{x}\right) + \frac{1}{4}\cos\left(\frac{2\pi}{\vec{T}'}\vec{x} + \delta\right) + \frac{1}{8}\left[\cos 2\pi\left(\frac{2}{\vec{T}'}\right) + \cos 2\pi\left(\frac{2}{\vec{T}'}\right)\left(\vec{x} - \frac{1}{2}\delta\right)\right]. \tag{16}$$

The average intensity of the waveform is calculated as

$$I_{\text{aver}} = \frac{1}{\vec{T}'}\int_0^{\vec{T}'} r' \mathrm{d}\vec{x} = \frac{1}{8}\cos\left(\frac{2\pi}{\vec{T}'}\delta\right) + \frac{1}{4}. \tag{17}$$

In figure 2(f), two waveforms which are on different cross-sections along the orientation of the real moiré case with a different angular displacement δ have been presented. It is obvious that their average intensities are different from each other. The average intensity of the different waveforms in the real moiré case is changing periodically with the variation of δ.

(2) The pseudo-moiré case:

In formula (11), we have $\vec{T}'_1 / \vec{T}'_2 = n/m$. Then

$$r' = \frac{1}{4} + \frac{1}{4}\cos\left(\frac{2\pi}{\vec{T}'}\vec{x}\right) + \frac{1}{4}\cos\frac{2\pi n}{m\vec{T}'}(\vec{x} + \delta) + \frac{1}{8}\left[\cos 2\pi\frac{m+n}{m\vec{T}'}\left(\vec{x} + \frac{n}{m+n}\delta\right) + \cos 2\pi\frac{m-n}{m\vec{T}'}\left(\vec{x} - \frac{n}{m-n}\delta\right)\right]. \tag{18}$$

The upper limit of the integration can be chosen as the least common multiple of $\vec{T}'_1$ and $\vec{T}'_2$. Then the average intensity of the waveform is calculated from

$$I_{\text{aver}} = \frac{1}{\vec{T}'}\int_0^{\vec{T}'} r' \,\mathrm{d}\vec{x} = \frac{1}{4}. \tag{19}$$

In figure 2(g), two waveforms which are on different cross-sections along the orientation of the pseudo-moiré case with the different angular displacements δ have been presented. The two average intensities of the two curves are the same. According to the above discussion, when the average intensity of the generated moiré waveform r' is changing with the parameter δ, the moiré form is a real moiré form. But when the average intensity keeps constant, it generates a pseudo-moiré form. The real moiré and pseudo-moiré forms can be distinguished by the different average intensities in different period ratios.

The first conclusion is proposed: that the different ratios of the two equivalent periods result in the illusive discrimination of the human visual system for the average intensity of the generated waveforms in the multiplicative superposition. This can be actually boiled down to the microstructure versus the macrostructure effects. The variations of the intensity and the average intensity in the microstructure in different situations make the human eyes produce confusion of the average intensity of the moiré waveform in the macrostructure. According to the facts, the Fourier analysis cannot obtain the local variation of the intensity or the average intensity in the microstructure (one period or several periods) of the superposition. But the variation can be observed by the human visual system.

When the ratio of the two equivalent periods is equal to 1, the variations of intensity and average intensity in the microstructure captured by human eyes do not influence the angular displacement effects. Then the average intensity of the newly generated waveform will change with the angular displacement. If the period of the generated waveform falls into the visual area of the human eyes, the real moiré form appears.

When the ratio is not equal to 1, the variations of intensity and average intensity in the microstructures, which are connected by human eyes into the moiré-like band contribute different operations to the phenomenon. The effect on the average intensity introduced by the angular displacement will be canceled by it. The angular displacement only modifies the shape of the waveform and does not influence the average intensity which keeps constant. But at the moment, the human visual system still considers that the angular displacement is displayed. When the period of the generated waveform falls into the visual area of human eyes, the confusion will make the pseudo-moiré form appear.

Another conclusion can also be obtained from the analysis. Namely, the real and pseudo-moiré cases may coexist and appear in the same superposition. Figure 2(h) shows the superposition $r_1 \times r_2$ in the image. Both the real and pseudo-moiré cases in the same superposition have been observed simultaneously by our eyes in two directions. The periods of the generated waveforms of different moiré cases are calculated. The period T_{r} is equal to 2.49 and the period T_{p} is equal to 2.13. So when the condition $T_{\text{r}} \approx T_{\text{p}}$ is satisfied, real moiré and pseudo-moiré coexistence appears. More detailed analysis of the coexistence of real and pseudo-moiré cases will be discussed in section 5.

3. Theoretical interpretation for the multiplicative superposition of binary gratings

3.1. Description of the generated moiré case by using the Fourier expansion

The two-sided Fourier expansion of the binary gratings r_i is

$$r_i = \sum_{m=-\infty}^{\infty} a_m \cos(2\pi m(x\cos\theta_i + y\sin\theta_i)/T_i),$$

$$\text{where } a_{0i} = \frac{\tau_i}{T_i}, \quad a_m = \frac{1}{m\pi}\sin\left(\frac{\pi m\tau_i}{T_i}\right). \tag{20}$$

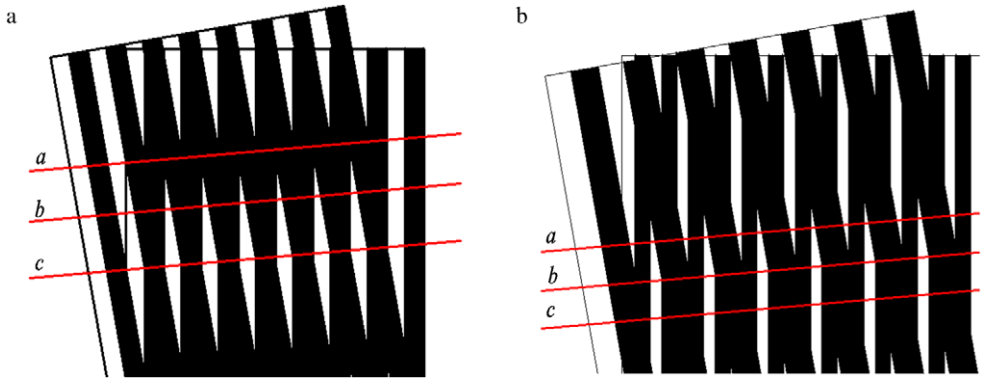

Figure 3. Different moiré phenomena in the multiplicative superposition of binary gratings. The lines a, b and c are along the direction of each generated moiré form. (a) The real moiré form whose relationships satisfy $T_1{:}T_2 = 1{:}1$ and $\tau_1/T_1 = \tau_2/T_2 = 1/2$. (b) The pseudo-moiré form whose relationships satisfy $T_1{:}T_2 = 1{:}2$ and $\tau_1/T_1 = \tau_2/T_2 = 1/2$.

A vector notation has been used for the generalization of expression (20):

$$r_i = \sum_{m=-\infty}^{\infty} a_m \cos\left(\frac{2\pi}{\vec{T}_i}\vec{x}\right), \qquad \text{where}$$
$$\vec{T}_i = \frac{(\cos\theta_i, \sin\theta_i)}{T_i} \text{ and } \vec{x} = (x, y). \tag{21}$$

The multiplicative superposition is

$$r_m = r_1 \times r_2 = \frac{1}{2}\sum_{m=-\infty}^{+\infty}\sum_{n=-\infty}^{+\infty} a_m^1 a_n^2 \times \cos 2\pi \vec{x}\left(\frac{m}{\vec{T}_1} + \frac{n}{\vec{T}_2}\right) + \frac{1}{2}\sum_{m=-\infty}^{+\infty}\sum_{n=-\infty}^{+\infty} a_m^1 a_n^2 \cos 2\pi \vec{x}\left(\frac{m}{\vec{T}_1} - \frac{n}{\vec{T}_2}\right). \tag{22}$$

The $(k_1, \pm k_2)$ moiré form is isolated as

$$m_{k_1,k_2} = \frac{1}{2}\sum_{n'=-\infty}^{+\infty} a_{n'k_1}^1 a_{n'k_2}^2 \cos 2\pi n' \vec{x}\left(\frac{k_1}{\vec{T}_1} \pm \frac{k_2}{\vec{T}_2}\right),$$

$$\text{where } \begin{cases} a_{n'k_1}^1 = \dfrac{1}{n'k_1\pi}\sin\left(\dfrac{\pi n' k_1 \tau_1}{T_1}\right) \\ a_{n'k_2}^2 = \dfrac{1}{n'k_2\pi}\sin\left(\dfrac{\pi n' k_2 \tau_2}{T_2}\right). \end{cases} \tag{23}$$

(1) $k_1 = k_2$.

The generated moiré form is the $(1, \pm 1)$ moiré one. Then we have

$$a_1^1 = \frac{1}{\pi}\sin\left(\frac{\pi\tau_1}{T_1}\right) \qquad \text{and}$$
$$a_1^2 = \frac{1}{\pi}\sin\left(\frac{\pi\tau_2}{T_2}\right). \tag{24}$$

Because the conditions $0 < \tau_1/T_1 < 1$ and $0 < \tau_2/T_2 < 1$ are always satisfied, a_1^1 and a_1^2 are not equal to 0. The $(1, \pm 1)$ moiré cases are always the real moiré cases, no matter what the opening ratio is.

Table 1. The 'and' operation.

Operation	0 and 0	0 and 1	1 and 0	1 and 1
Intensity value	0	0	0	1

(2) $k_1 \neq k_2$.

When $n'k_1\tau_1/T_1 = N$ or $n'k_2\tau_2/T_2 = N$ (N is an arbitrary integer), $a_{n'k1}^2$ or $a_{n'k2}^2$ will be equal to 0. This makes the $(k_1, \pm k_2)$ moiré form be like the pseudo-moiré one. In contrast, the $(k_1, \pm k_2)$ moiré forms are real moiré forms when both $a_{n'k1}^2$ and $a_{n'k2}^2$ are not equal to 0.

3.2. The physical meaning of the interpretation

The difference between the cosinusoidal and binary gratings is that there only exist two values '0' and '1' in the binary grating. So a concept will be firstly introduced to illustrate the multiplicative superposition of two binary gratings. The multiplicative superposition is actually the operation 'and' which is shown in table 1.

It is very much more difficult to calculate the average intensity of the moiré case for the binary gratings than for the cosinusoidal gratings. To solve the problem, the following examples in figure 3 will be used instead of the complicated derivation, which is visualized enough to prove the validity of our interpretation.

In fact, the average intensity of the grating can be expressed by the duty ratio of the length of the white (the value is '1') line and the total length of the line. From figure 3(a), the average intensities of the lines a, b and c are completely different from each other. In the contrast of figure 3(a), the average intensity in a, b and c in figure 3(b) keeps constant. It is easy to see that the duty ratio is changing periodically in the real moiré case but keeps constant in the pseudo-moiré case, which proves the conclusion in section 2.3. So a similar interpretation can also be used for two binary gratings in the multiplicative superposition.

Because the average intensity in different lines which parallels the orientation of the pseudo-moiré form is

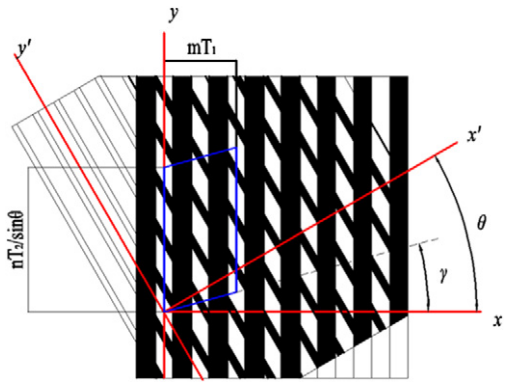

Figure 4. Schematic of the pseudo-moiré case for the calculation of the average intensity.

invariable, the average intensity of the pseudo-moiré form can be calculated from the ratio of the white area and the total area of the parallelogram which is enclosed by the blue line in figure 4.

The average intensity can be expressed as

$$I_{\text{aver}} = S_{\text{w}}/S_{\text{total}} = (\tau_1/T_1)/(\tau_2/T_2), \tag{25}$$

where $S_{\text{total}} = mT_1 \times (nT_2/\sin\theta)$ and $S_{\text{w}} = m\tau_1 \times (n\tau_2/\sin\theta)$. S_{w} is the area of the white part of the parallelogram, and S_{total} is the total area of the parallelogram. Therefore, the average intensity of the pseudo-moiré form in the multiplicative superposition for the two binary gratings is always equal to the product of the two opening ratios $(\tau_1/T_1)(\tau_2/T_2)$.

4. Theoretical interpretation for additive superposition

The additive superpositions of the cosinusoidal gratings and the binary gratings are given by

$$\vec{r}_m = \frac{\vec{r}_1 + \vec{r}_2}{2} = \tfrac{1}{4}\left(\cos(2\pi \vec{f}_1 \cdot \vec{x}) + \cos(2\pi \vec{f}_2 \cdot \vec{x})\right) + \tfrac{1}{2}, \tag{26}$$

and

$$\vec{r}_m = \frac{\vec{r}_1 + \vec{r}_2}{2} = \frac{1}{2}\left(\sum_{m=-\infty}^{\infty} a_m \cos\left(\frac{2\pi}{\vec{T}_1}\vec{x}\right) + \sum_{m=-\infty}^{\infty} a_n \cos\left(\frac{2\pi}{\vec{T}_2}\vec{x}\right)\right). \tag{27}$$

In formulas (4) and (22), the pseudo-moiré terms are the terms whose values are zero but that do exist in the multiplicative superposition. In contrast, there is no new term with new periods generated, only integer multiples of the original terms in the additive superposition. So the pseudo-moiré terms are really non-existent. This proves that all moiré phenomena accepted by human eyes are pseudo-moiré ones in the additive superposition.

An interesting conclusion can be derived from figure 5. The additive superposition is likely reversed from the multiplicative superposition for the same gratings r_1 and r_2. It is apparent in the superposition of the binary gratings. So the direction of the moiré phenomenon in the additive superposition is the same as in the multiplicative superposition.

Table 2. The 'or' operation.

Operation	0 or 0	0 or 1	1 or 0	1 or 1
Intensity value	0	1	1	1

Analysis similar to that of section 2.3 is adopted for the cosinusoidal gratings.

The average intensities of waveforms in vertical cross-sections, which are along two directions of the moiré case accepted by our eyes, remain constant in the superposition of $r_1 + r_2$ in figure 6. As in the interpretation of section 2.3, these two moiré forms received are the pseudo-moiré ones. The variation and average intensity in the microstructure introduce the illusional discrimination to human eyes.

There are some differences between binary gratings and cosinusoidal gratings in the additive superposition. An operation 'or' (as in table 2) opposite to the operation 'and' in section 3.2 is introduced to illustrate this.

In figure 5(d), the average intensity in different lines along the direction which is the same as for the real moiré form in $r_1 \times r_2$ is varying periodically. This seems not in accord with our interpretation. In fact, the difference is introduced by the characteristic of the binary gratings. The duality '0' and '1' in the binary grating alters the distribution of the intensity and the average intensity in the microstructure. At the moment, the discrete property of the binary grating does not display the same effect as was introduced by the cosinusoidal gratings. It makes the average intensity of the pseudo-moiré form still varying. Oppositely to this, the graded value distribution of the cosinusoidal gratings will not modify the average intensity of the moiré case. This is determined by the particularity of the binary gratings. The corresponding phenomenon can be judged by the Fourier expansion and explained by the above interpretation with definite amendment. It does not impact the validity of our interpretation.

5. Discussion of the coexistence of the real moiré and pseudo-moiré cases

In sections 2 and 3, the coexistence of real and pseudo-moiré cases in the multiplicative superposition of cosinusoidal gratings—the binary gratings—has been proved. In Kong's study [8], the situation for the cosinusoidal gratings has been discussed. The conclusion is that when T_2/T_1 approaches 1, the real moiré case is more prominent; when T_2/T_1 approaches 2, the pseudo-moiré case becomes more prominent; when $T_2/T_1 = 1.5$, them seem equal to human eyes.

The special characteristic in the binary grating superposition is that the appearance of different moiré forms depends on not only the periods but also the opening ratios, so the

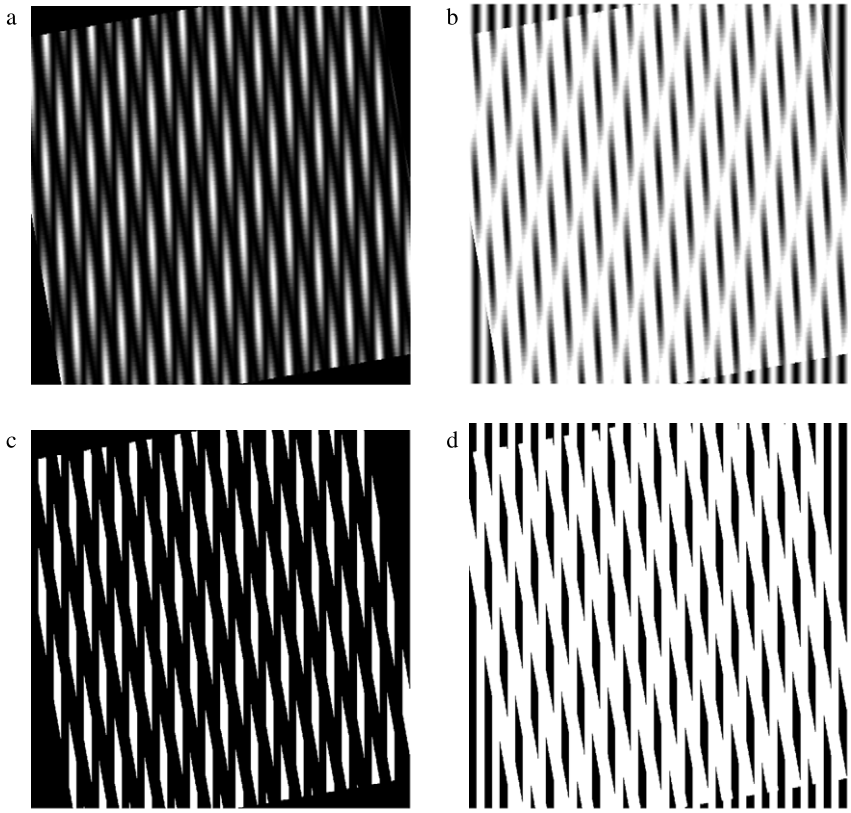

Figure 5. Schematic of the multiplicative superposition and the additive superposition. The left column is in the multiplicative superposition and the right column is in the additive superposition. (a) The multiplicative superposition of $r_1 \times r_2$. (b) The additive superposition of $r_1 + r_2$. $r_1 = 1/2\cos[(\pi/10)(x\cos(0) + y\sin(0))] + 1/2$, $r_2 = 1/2\cos[(\pi/15)(x\cos(\pi/18) + y\sin(\pi/18))] + 1/2$. (c) The multiplicative superposition of $r_1 \times r_2$. (d) The additive superposition of $r_1 + r_2$. $r_1(x, y) = \sum_{n=-\infty}^{\infty} a_n^{(1)} \cos(\frac{2\pi nx}{40})$, $r_2(x, y) = \sum_{n=-\infty}^{\infty} a_n^{(2)} \cos(\frac{2\pi n}{20}(x\cos(\frac{\pi}{18}) + y\sin(\frac{\pi}{18})))$, $\frac{\tau_1}{T_1} = \frac{\tau_2}{T_2} = \frac{1}{2}$.

situation is complicated. In our following example, we have $T_1 = 36$, $T_2/T_1 = m/n = k$:1 ($k \geq 1$ and k is a rational number) and $\theta = 10°$. The opening ratio of r_1 is chosen as $1/2$. This is because whatever the opening ratio of r_1 is, $a_{n'k1}^2$ is not equal to zero in our assumption $T_2/T_1 = k$:1. This can simplify the discussion without influencing the conclusion.

(1) $1 < k < 1.5$: when $\tau_2/T_2 = 1/2$, there will be generated the (1, ±2) moiré case which is a pseudo-moiré one. The examples in figures 7(a) and (b) are in the circumstance $k = 1.1$. The conclusion is obtained that the real moiré case is always dominant in the generated moiré case no matter what the opening ratio is, when $1 < k < 1.5$.

(2) $k = 1.5$: figures 7(c) and (d) satisfy the condition $k = 1.5$. When $\tau_2/T_2 = 1/2$, the real moiré and pseudo-moiré cases coexist in (c). But the real moiré case is dominant when $\tau_2/T_2 \neq 1/2$ in (d).

(3) $1.5 < k < 2$: figures 7(e) and (f) are for the circumstance of $k = 1.9$. The pseudo-moiré case is dominant in (e) when $\tau_2/T_2 = 1/2$. In (f), the real moiré case is dominant when $\tau_2/T_2 \neq 1/2$.

(1) In figures 8(a) and (b), $k = 2.5$. The pseudo-moiré conditions are satisfied. The superposition presents the coexistence of pseudo-moiré and real moiré cases.

(2) In figures 8(c) and (d), the period ratio is $2 < k = 2.25 < 5/2$, and the pseudo-moiré case is dominant when $\tau_2/T_2 = 1/2$, but the real moiré case is dominant when $\tau_2/T_2 = 1/3$. In figures 8(e) and (f), the period ratio is $5/2 < k = 2.75 < 3$, and the situation is the contrary.

According to the above analysis, the following conclusion can be produced. Here we have $N < k < N + 1$ ($N > 1$ and N is an arbitrary integer) and $\tau_2/T_2 = r/s$ (r and s are integers and irreducible with respect to each other).

$N < k < (2N+1)/2$: when $s = N$, the pseudo-moiré case is dominant. In other cases, the real moiré case is dominant.

$k = (2N + 1)/2$: when $s = N$ or $s = N + 1$, pseudo-moiré and real moiré cases are coexisting. In other cases, the real moiré form is dominant.

$(2N+1)/2 < k < N+1$: when $s = N+1$, the pseudo-moiré case is dominant. In other cases, the real moiré case is dominant.

$k = N$ or $N + 1$: when the conditions $s = N$ and $k = N$ or $s = N + 1$ and $k = N + 1$ are satisfied, there only exists the pseudo-moiré case. Otherwise, the real moiré case is dominant.

The calculated parameters of figure 8 are listed in table 3.

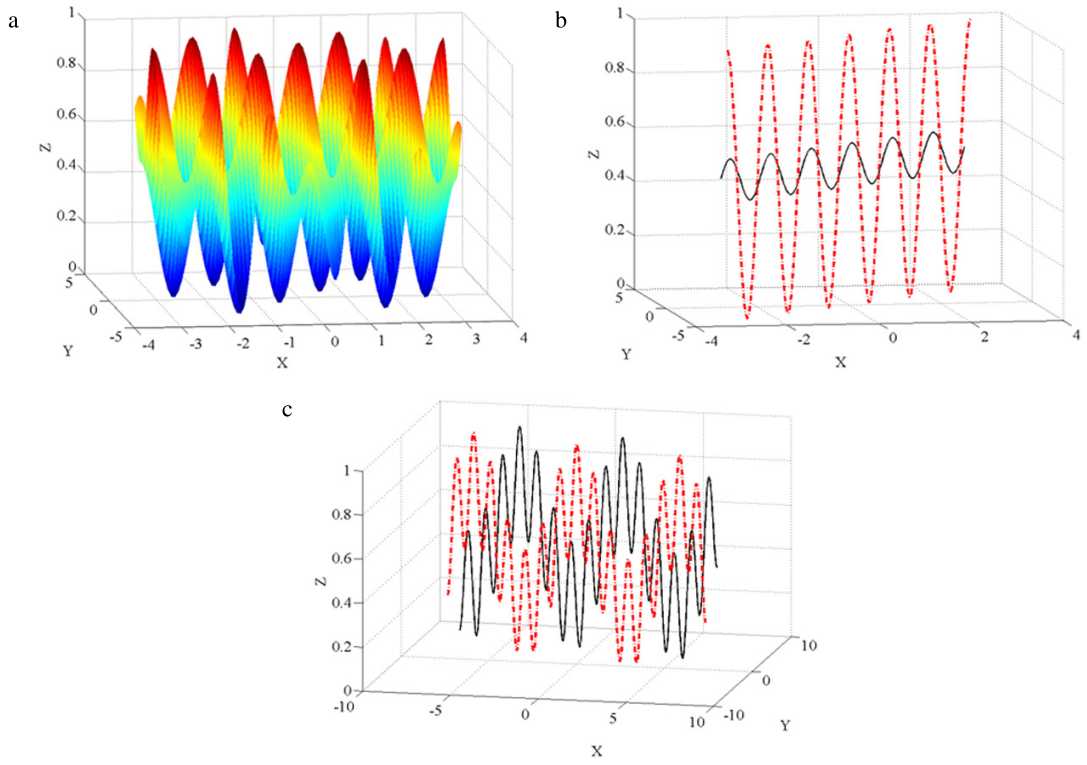

Figure 6. The oscillograms and the waveforms in vertical cross-sections in the additive superposition. (a) The wave profile of $r_1 + r_2$. (b) The waveform along $\cos\gamma_r$. (c) The waveform along $\cos\gamma_p$.

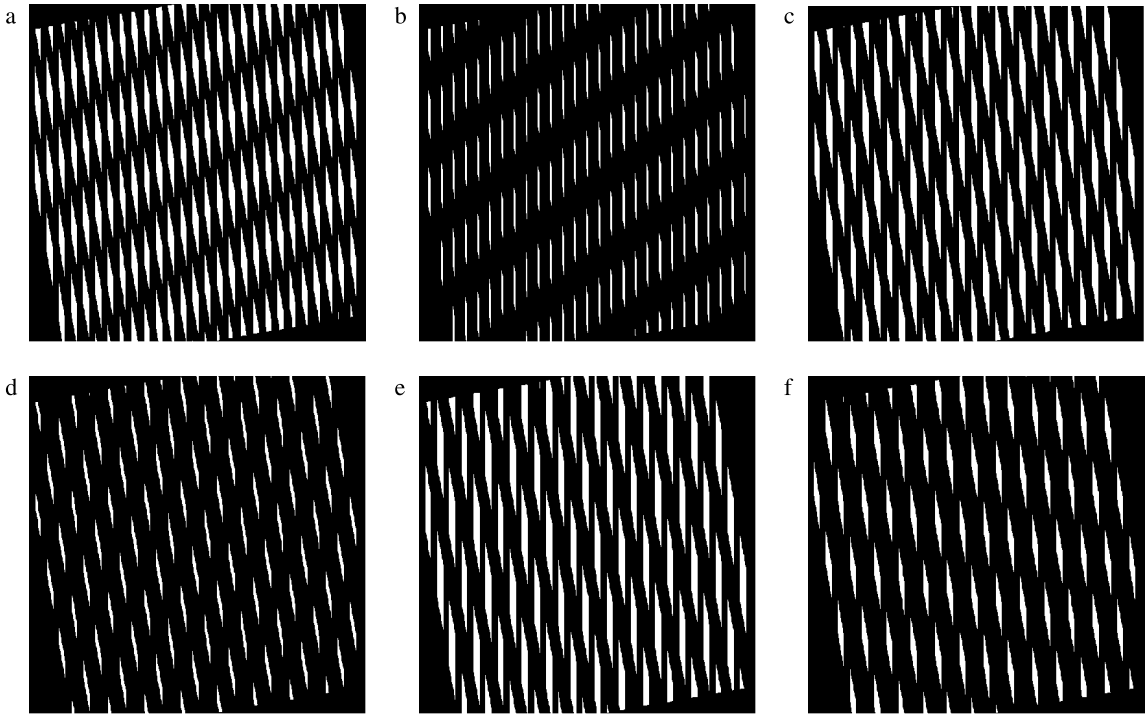

Figure 7. The multiplicative superposition of two slightly inclined binary gratings with period ratio $1 \leq k < 2$. (a) $k = 1.1$, $\tau_1/T_1 = 1/2$, $\tau_2/T_2 = 1/2$. (b) $k = 1.1$, $\tau_1/T_1 = 1/2$, $\tau_2/T_2 = 1/6$. (c) $k = 1.5$, $\tau_1/T_1 = 1/2$, $\tau_2/T_2 = 1/2$. (d) $k = 1.5$, $\tau_1/T_1 = 1/2$, $\tau_2/T_2 = 1/6$. (e) $k = 1.9$, $\tau_1/T_1 = 1/2$, $\tau_2/T_2 = 1/2$. (f) $k = 1.9$, $\tau_1/T_1 = 1/2$, $\tau_2/T_2 = 1/4$.

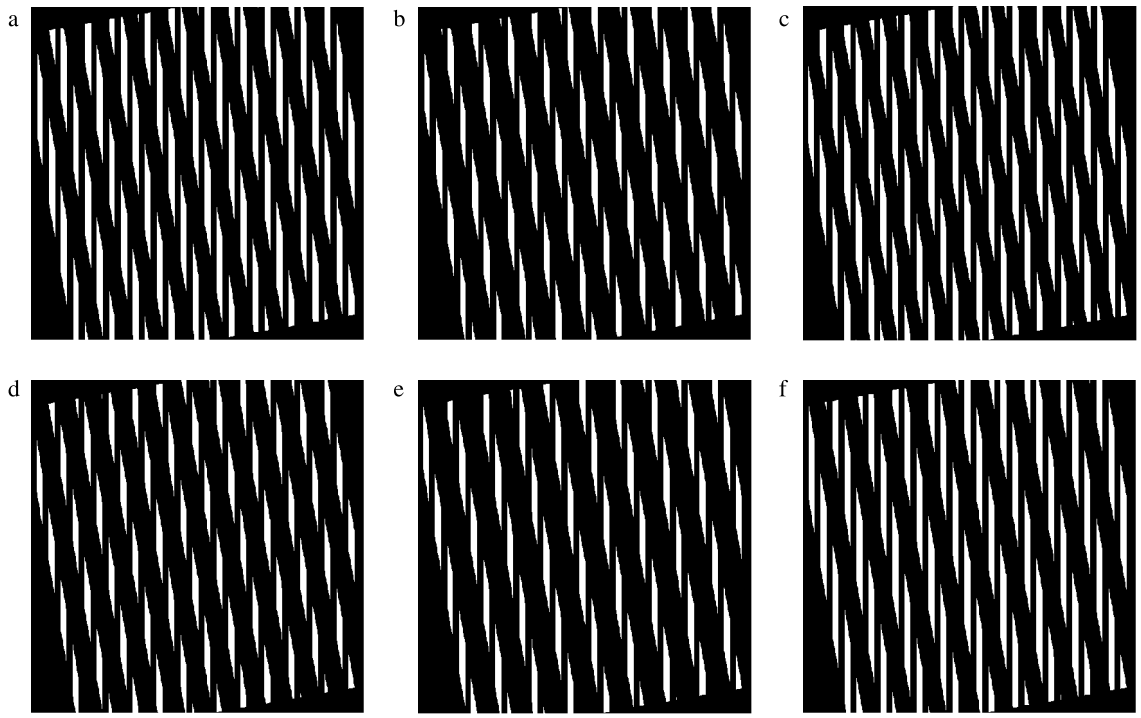

Figure 8. The multiplicative superposition of two slightly inclined binary gratings with period ratio $1 \leq k < 2$. (a) $k = 2.5$, $\tau_1/T_1 = 1/2$, $\tau_2/T_2 = 1/2$. (b) $k = 2.5$, $\tau_1/T_1 = 1/2$, $\tau_2/T_2 = 1/3$. (c) $k = 2.25$, $\tau_1/T_1 = 1/2$, $\tau_2/T_2 = 1/2$. (d) $k = 2.25$, $\tau_1/T_1 = 1/2$, $\tau_2/T_2 = 1/3$. (e) $k = 2.75$, $\tau_1/T_1 = 1/2$, $\tau_2/T_2 = 1/3$ and (f) $k = 2.75$, $\tau_1/T_1 = 1/2$, $\tau_2/T_2 = 1/2$.

Table 3. Parameters of the real and pseudo-moiré cases in figure 8.

Period ratio	Opening ratio of r_2	Real moiré case	Pseudo-moiré case
2.5	1/2	$\cos\gamma_r = 0.050$ $T_r = 25.794$	$\cos\gamma_p = 0.077$ $T_p = 20.076$
2.5	1/3	$\cos\gamma_r = 0.050$ $T_r = 25.794$	$\cos\gamma_p = 0.095$ $T_p = 16.426$
2.25	1/2	$\cos\gamma_r = 0.136$ $T_r = 63.427$	$\cos\gamma_p = 0.778$ $T_p = 181.44$
2.25	1/3	$\cos\gamma_r = 0.136$ $T_r = 63.427$	$\cos\gamma_p = 0.100$ $T_p = 15.486$
2.75	1/3	$\cos\gamma_r = 0.098$ $T_r = 55.815$	$\cos\gamma_p = 0.930$ $T_p = 176.479$
2.75	1/2	$\cos\gamma_r = 0.098$ $T_r = 55.815$	$\cos\gamma_p = 0.073$ $T_p = 20.920$

6. Conclusions

The Fourier expansion of the grating superposition, the geometric calculation in the image domain and the calculation of the average intensities of different moiré waveforms have been combined to present an appropriate interpretation for the real and pseudo-moiré phenomena, which are generated by two periodic cosinusoidal and binary gratings in the multiplicative and the additive superposition.

The interpretation considers newly generated terms in the Fourier expansion of the superposition as the expression for the moiré form. The method gives the criterion for distinguishing real and pseudo-moiré phenomena. By the geometric analysis in the image domain, important parameters which can define the real moiré and pseudo-moiré cases have been proposed. The analysis and calculation of the average intensity of the moiré form sufficiently interpret the generation of the visible moiré phenomenon. The microstructure versus macrostructure effect, namely the influence of the variation of the intensity and the average intensity in the microstructure, introduces the confusion of the average intensity in the macrostructure to human eyes in different ratios of equivalent periods.

The Fourier expansion analysis is also appropriate for the additive superposition. So our interpretation operates as effectively in the additive superposition as in the multiplicative superposition. Although some amendment should be added to it to deal with the particularity of the binary gratings, it does not impact the property of the interpretation. Furthermore, our proposed interpretation provides a unified and concise analysis for the visible moiré phenomenon both in the multiplicative superposition and in the additive superposition, regardless of whether two superposed gratings are periodic cosinusoidal gratings or binary gratings.

Acknowledgment

This research was supported by the National Natural Science Foundation of China (NSFC) under grant 41074126.

References

[1] Abolhassani M and Mirzaei M 2007 Unification of formulation of moiré fringe spacing in parametric equation and Fourier analysis methods *Appl. Opt.* **46** 7924–6
[2] Kohayashi S 1993 *Handbook on Experimental Mechanics* 2nd edn (Bethel: SEM)

[3] Patorski K 1993 *Handbook of the Moiré Fringe Technique* (Amsterdam: Elsevier)
[4] Rayleigh L 1874 On the manufacture and theory of diffraction-gratings *Phil. Mag.* **81** 81–93
[5] Lebanon G 2011 Variational approach to moiré pattern synthesis *J. Opt. Soc. Am.* A **18** 1371–82
[6] Amidror I 2009 *The Theory of the Moiré Phenomenon* (London: Springer)
[7] Amidror I and Hersch R D 1998 Fourier-based analysis and synthesis of moirés in the superposition of geometrically transformed periodic structures *J. Opt. Soc. Am.* A **15** 1100–13
[8] Patorske K, Yokozeki S and Suzuki T 1976 Moiré profile prediction by using Fourier series formalism *Japan. J. Appl. Phys.* **15** 443–56
[9] Amidror I and Hersch R D 2009 The role of Fourier theory and of modulation in the prediction of visible moiré effects *J. Mod. Opt.* **56** 1103–18
[10] Kong L, Cai S, Li Z, Jin G, Huang S, Xu K and Wang T 2011 Interpretation of moiré phenomenon in the image domain *Opt. Express* **19** 18399–409
[11] Patorski K, Pokorski K and Trusiak M 2011 Fourier domain interpretation of real and pseudo-moiré phenomena *Opt. Express* **19** 26065–78